The North Pacific Pacemaker Effect on Historical ENSO and Its Mechanisms

DILLON J. AMAYA

Scripps Institution of Oceanography, University of California, San Diego, La Jolla, California

YU KOSAKA

Research Center for Advanced Science and Technology, The University of Tokyo, Tokyo, Japan

WENYU ZHOU

Scripps Institution of Oceanography, University of California, San Diego, La Jolla, California

YU ZHANG

Physical Oceanography Laboratory, Qingdao Collaborative Innovation Center of Marine Science and Technology, Ocean University of China, and Qingdao National Laboratory for Marine Science and Technology, Qingdao, China, and Scripps Institution of Oceanography, University of California, San Diego, La Jolla, California

SHANG-PING XIE AND ARTHUR J. MILLER

Scripps Institution of Oceanography, University of California, San Diego, La Jolla, California

(Manuscript received 14 January 2019, in final form 15 July 2019)

ABSTRACT

Studies have indicated that North Pacific sea surface temperature (SST) variability can significantly modulate El Niño–Southern Oscillation (ENSO), but there has been little effort to put extratropical–tropical interactions into the context of historical events. To quantify the role of the North Pacific in pacing the timing and magnitude of observed ENSO, we use a fully coupled climate model to produce an ensemble of North Pacific Ocean–Global Atmosphere (nPOGA) SST pacemaker simulations. In nPOGA, SST anomalies are restored back to observations in the North Pacific (>15°N) but are free to evolve throughout the rest of the globe. We find that the North Pacific SST has significantly influenced observed ENSO variability, accounting for approximately 15% of the total variance in boreal fall and winter. The connection between the North and tropical Pacific arises from two physical pathways: 1) a wind–evaporation–SST (WES) propagating mechanism, and 2) a Gill-like atmospheric response associated with anomalous deep convection in boreal summer and fall, which we refer to as the summer deep convection (SDC) response. The SDC response accounts for 25% of the observed zonal wind variability around the equatorial date line. On an event-by-event basis, nPOGA most closely reproduces the 2014/15 and the 2015/16 El Niños. In particular, we show that the 2015 Pacific meridional mode event increased wind forcing along the equator by 20%, potentially contributing to the extreme nature of the 2015/16 El Niño. Our results illustrate the significant role of extratropical noise in pacing the initiation and magnitude of ENSO events and may improve the predictability of ENSO on seasonal time scales.

1. Introduction

El Niño–Southern Oscillation (ENSO) dominates interannual variability of the tropical Pacific coupled ocean–atmosphere system, impacting global weather and climate through atmospheric teleconnections (Horel and Wallace 1981). Historically, ENSO predictability research has focused on processes local to the tropics (e.g., Clarke 2014); however, over the past decade many studies have shown that mid- to high-latitude atmospheric variability can significantly influence ENSO evolution through ocean–atmosphere teleconnections (e.g., Vimont et al. 2001, 2009; Levine et al. 2017; Alexander et al. 2010). For example, stochastic fluctuations of the North

Corresponding author: Dillon J. Amaya, djamaya@ucsd.edu

DOI: 10.1175/JCLI-D-19-0040.1

Pacific Oscillation (NPO), a mode of atmospheric variability over the North Pacific (Rogers 1981), can initiate the so-called seasonal footprinting mechanism (SFM; Vimont et al. 2001). The SFM describes the weakening of the North Pacific trade winds during boreal winter by the southern lobe of the NPO. This forces an anomalous latent heat flux (Q_{LH}) and leaves a "footprint" of sea surface temperature (SST) anomalies (SSTAs) extending from the coast of Baja California southwestward into the tropics. These SSTAs persist into boreal summer due to reinforcing feedbacks between the SST and the overlying circulation through latent and shortwave heat fluxes (Vimont et al. 2003b, 2009). This ultimately drives anomalous convection and atmospheric circulation anomalies in the deep tropics that can potentially trigger ENSO through enhanced ocean forcing (Vimont et al. 2003a,b).

The southwestward propagation of SST anomalies is a potentially important component of the SFM and involves a series of interactions between surface wind anomalies, evaporation anomalies, and SSTAs. These coupled interactions, known as wind–evaporation–SST (WES) feedback (Xie and Philander 1994), signal the development of a Pacific meridional mode (PMM) event (Chiang and Vimont 2004). For a positive PMM event and for positive WES feedback in the Northern Hemisphere, the anomalous atmospheric response to warm SSTAs includes southwesterly flow on the southwestern edge of the maximum SST, which further weakens the northeasterly trades, producing an anomalous Q_{LH} that warms the ocean at that location. The net result is a southwestward propagation of the SSTAs and surface wind anomalies, which act to teleconnect ocean–atmosphere surface anomalies from the subtropics into the deep tropics (Liu and Xie 1994; Chiang and Vimont 2004; Vimont 2010; Martinez-Villalobos and Vimont 2017). While the southwestward propagation of SSTAs through the PMM appears to be an important component of the SFM, it is not clear whether such propagation is essential; in particular, it is possible that subtropical SSTAs themselves may be sufficient to excite a response in the tropics that can lead to ENSO variability. One intent of this study is to examine the possibility of a direct-forced tropical response to subtropical North Pacific SSTAs.

Several studies have attempted to quantify the extent to which North Pacific ocean–atmosphere variability can act as a precursor and predictor of ENSO. Vimont et al. (2003a) use a triad of global climate model (GCM) simulations to show that the SFM accounted for 20%–40% of the model's interannual ENSO variability. Chang et al. (2007) use observational reanalysis data to suggest 12 out of the 17 ENSO events from 1958 to 2000 were preceded by PMM conditions in the subtropical North Pacific. Larson and Kirtman (2014) analyze a set of hindcasts from the North American Multimodel Ensemble and show some skill at predicting east Pacific El Niño events when initialized with positive PMM conditions. Furthermore, Lu et al. (2017) show considerable skill in reproducing model ENSO when assimilating extratropical winds in a perfect-model framework. In forecast models, the PMM induced by internal variability of the extratropical atmosphere is an important source of uncertainty in predicting equatorial SSTs during the boreal spring (Ma et al. 2017).

These previous studies have advanced our understanding of the complex relationship between North Pacific SST variability and ENSO; however, there are still a variety of limitations that must be overcome in order to improve seasonal predictability of ENSO. For example, many PMM/ENSO studies are based on idealized climate model simulations with simplified or reduced model physics (Zhang et al. 2009; Alexander et al. 2010; Zhang et al. 2014b; Lu et al. 2017), which do not necessarily characterize the full extent of observed internal variability. In contrast, studies that have restricted themselves to observational reanalysis products suffer from reduced degrees of freedom given the limited observational record (Chang et al. 2007; Min et al. 2017). To overcome a limited sample size, several studies have analyzed long preindustrial control simulations (Shin and An 2018; Sanchez et al. 2019); however, such methods must still contend with model biases in the tropical and North Pacific regions. Finally, there has been little effort to put North Pacific precursors in the context of the real-world ENSO events (Larson and Kirtman 2014; Lu and Liu 2018).

A reasonable approach to rectify many of these issues is to conduct a North Pacific SST pacemaker experiment. In a pacemaker experiment, a climate model is forced by the observed trajectory of SST in a specific region of the world's oceans, while allowing the model to freely evolve everywhere else (e.g., Deser et al. 2017). Forcing the model with observations ensures the model "sees" realistic variability free of model biases. The additional degrees of freedom afforded by an ensemble of these simulations also make it possible to more accurately quantify the influence of regional SST variability on the observed time evolution of the climate system. Such multimember pacemaker experiments have been successfully used to analyze real-world teleconnections from the tropical Pacific (Kosaka and Xie 2013; Deser et al. 2017; Zhang et al. 2018) and from the North (Levine et al. 2017) and tropical Atlantic (Li et al. 2016).

In this study, we present the first North Pacific pacemaker experiment designed to investigate the connection

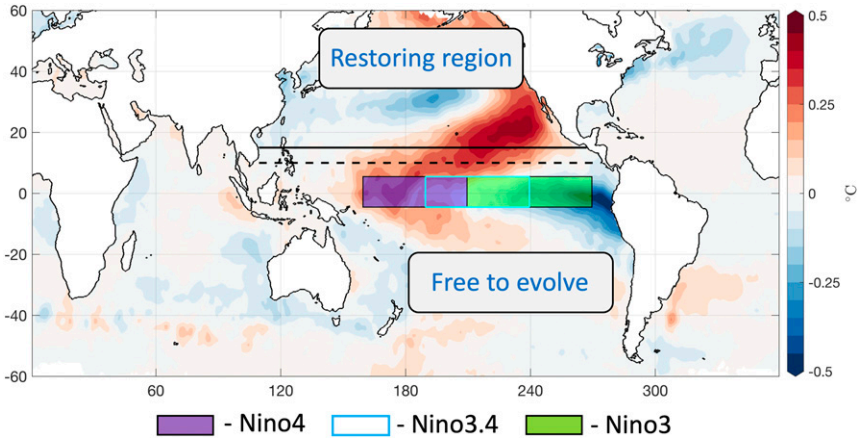

FIG. 1. North Pacific Ocean–Global Atmosphere (nPOGA) experimental design. SSTs are restored to the model climatology plus observed historical anomaly in the Pacific Ocean north of 15°N (solid black line). There is a 5° linearly decreasing buffer zone from 15° to 10°N (dashed black line). Colored shading represents HadISST SSTAs regressed on the PMM_{CV} index. Shaded boxes indicate different Niño indices used in this study.

between the North Pacific and ENSO in observations. We find that pacing the model with North Pacific SST provides significant skill in reproducing observed ENSO, especially in boreal fall and winter. These midlatitude teleconnections are made possible through a combination of WES feedback-driven propagation in boreal spring, and a secondary pathway related to an interaction between North Pacific SSTAs and the mean intertropical convergence zone (ITCZ). On an event-by-event basis, the clearest examples of the North Pacific influence on ENSO are the weak 2014/15 El Niño and the extreme 2015/16 El Niño. In particular, our results suggest that North Pacific SSTAs would have driven a more coherent 2014/15 El Niño than observed if not for internal variations of tropical surface winds. Further, we find that equatorial wind forcing associated with the extreme 2015/16 was significantly enhanced by the strongest North Pacific PMM event in at least the last 70 years. Our results take an important step toward quantifying North Pacific teleconnections within the context of historical ENSO events, and highlight the importance of recognizing the distinct pathways by which extratropical ocean–atmosphere variability can teleconnect into the tropics and influence ENSO.

The rest of this paper is organized as follows. In section 2, we outline the experimental design of our model simulations and the observational datasets used. Sections 3 and 4 assesses the pacemaker's ability to produce a physically consistent connection between the North Pacific and the tropics. Section 5 discusses individual El Niño events, and section 6 provides a summary with conclusions.

2. Data and methods

a. Model description

In this study, we use the Geophysical Fluid Dynamics Laboratory coupled model, version 2.1 (Delworth et al. 2006; GFDL-CM2.1). GFDL-CM2.1 has land and atmosphere components with a horizontal resolution of ~2° latitude × 2.5° longitude and 24 vertical levels. The atmosphere model (GFDL-AM2.1) can be run as an uncoupled component by prescribing the lower boundary condition. The ocean has 50 vertical levels and a horizontal resolution of 1° for both latitude and longitude, with meridional resolution equatorward of 30° becoming progressively finer until it is 1/3° at the equator.

b. nPOGA and nATMO experimental design

To quantify the role of North Pacific SSTs in pacing the timing and magnitude of past ENSO events, we use GFDL-CM2.1 to produce an ensemble of North Pacific Ocean–Global Atmosphere (nPOGA) pacemaker simulations (Fig. 1). In nPOGA, SSTs north of 15°N in the Pacific are restored to the model climatology plus the observed anomaly calculated from the Hadley Centre Global Sea Ice and Sea Surface Temperature, version 1.1 (HadISST), dataset (Rayner et al. 2003). The model climatology is based on the 1920–2005 average daily climatology of 10 fully coupled historical simulations, each forced with historical radiative forcing from phase 5 of the Coupled Model Intercomparison Project (CMIP5; Taylor et al. 2012). Observed anomalies are based on monthly values that are linearly interpolated to daily before restoration.

The SST restoration is done by overriding the surface sensible heat flux to the ocean (F) where

$$F = (1-\alpha)F_* + \alpha\frac{c\rho D}{\tau}(\mathrm{SST}' - \mathrm{SST}'_*). \quad (1)$$

Primes denote anomalies, asterisks represent model-diagnosed values, c is the specific heat of seawater, ρ is the density of seawater, $D = 50$ m is the typical depth of the ocean mixed layer, and $\tau = 10$ days is the restoring time scale. The reference temperature (SST′) indicates the HadISST anomaly. The weighting coefficient (α) ranges from 0 to 1, where 1 is full restoration and 0 is no restoration. In Fig. 1, $\alpha = 1$ within the Pacific Ocean north of 15°N (solid black line). This value linearly decreases in a 5° buffer zone to $\alpha = 0$ south of 10°N in the Pacific (dashed line), and it is identically 0 everywhere else on the globe. nPOGA consists of a 10-member ensemble for 1950–2016. In addition to SST restoration, each member is initialized with slightly different initial conditions and forced with CMIP5 radiative forcings for 1950–2005 and representative concentration pathway (RCP4.5) for 2006–16.

It is important to assess whether atmospheric variability *outside* of the restoring region in nPOGA is the result of local tropical coupled feedbacks or is merely a "downstream" response to restored North Pacific SSTs. To isolate the influence of coupled feedbacks, we compare nPOGA to a 10-member ensemble of North Pacific, atmosphere-only (nATMO) runs. Ensemble members in nATMO use GFDL-AM2.1 in uncoupled mode and are forced with the same historical + RCP4.5 radiative forcings as nPOGA. Additionally, the lower boundary condition is set to the same SST values as nPOGA in the North Pacific (Fig. 1), and the model climatological seasonal cycle everywhere else. Therefore, the ensemble mean of nATMO represents the direct SST driven response independent of tropical coupled feedbacks.

Finally, in section 3 we compare nPOGA to the 10-member GFDL-CM2.1 historical+RCP4.5 simulation (HIST) available in the CMIP5 archive (https://esgf-node.llnl.gov/projects/cmip5/). HIST is forced by the same radiative forcings, but its internal variability is not constrained by the observations as in nPOGA. Therefore, we treat HIST as our control for this study.

c. Observational datasets and significance testing

The nPOGA and nATMO simulated results are compared to HadISST and the Japanese 55-year Reanalysis (JRA-55; 1.25° × 1.25°; Kobayashi et al. 2015). Comparisons between nPOGA/nATMO and JRA-55 are limited to their overlapping time periods (1958–2016). Results are qualitatively unchanged if we use the National Centers for Environmental Prediction–National Center for Atmospheric Research (NCEP–NCAR) reanalysis dataset for 1950–2016. In section 4, we perform a composite analysis on the standardized Chiang and Vimont (2004) PMM SST principal component ($\mathrm{PMM_{CV}}$ index) in observations, which is made available by the Earth System Research Laboratory (ESRL; https://www.esrl.noaa.gov/psd/data/timeseries/monthly/PMM/). For clarity, all datasets have been detrended, subjected to a 3-month running mean, and interpolated to the GFDL-CM2.1 atmospheric grid. Results are insensitive to changes in these data processing steps. Unless otherwise noted, statistical significance is determined using a Student's t test at the 95% confidence level after correcting the degrees of freedom for lag-1 autocorrelation.

3. Comparing simulated ENSO to observations

To assess nPOGA's ability to simulate real-world ENSO events, we compare area averaged Niño indices (Fig. 1 shaded boxes) in nPOGA and HadISST (Fig. 2). The full time series correlations between observed and simulated ensemble mean ENSO are $R = 0.25$, 0.31, and 0.34 for Niño-3, Niño-3.4, and Niño-4, respectively. The latter two correlations are significant at the 80% confidence level. While these correlations are not strongly significant, the values compare well to correlations of the same observed indices with our control experiment ($R = -0.01$, -0.01, and 0.01; not shown). nPOGA's skill is more readily apparent when comparing seasonally averaged correlations (Fig. 3). The HIST control simulation does not significantly reproduce observed ENSO variability in any season (not shown); however, nPOGA produces a 95% significant correlation with observed Niño-3 from September to January and with observed Niño-3.4 and Niño-4 from August to April. The persistent skill in the west/central Pacific (i.e., Niño-4 region) throughout the year is interesting, and suggests that the North Pacific SST-forced variability is more closely related to central Pacific (CP) ENSO than east Pacific events, which is consistent with previous studies (Furtado et al. 2012; Vimont et al. 2014; Lin et al. 2015).

Are nPOGA simulated ENSO events preceded by observed PMM events as we might expect? Figure 4 shows scatterplots of October–December (OND) Niño indices for the nPOGA ensemble mean (y axis) and HadISST (x axis). The shading of each circle denotes the magnitude of $\mathrm{PMM_{CV}}$ in the *preceding* February–April (FMA). Consistent with Fig. 3, there is a significant positive relationship between nPOGA simulated ENSO and observed ENSO ($R = 0.38$, 0.40, and 0.39 for

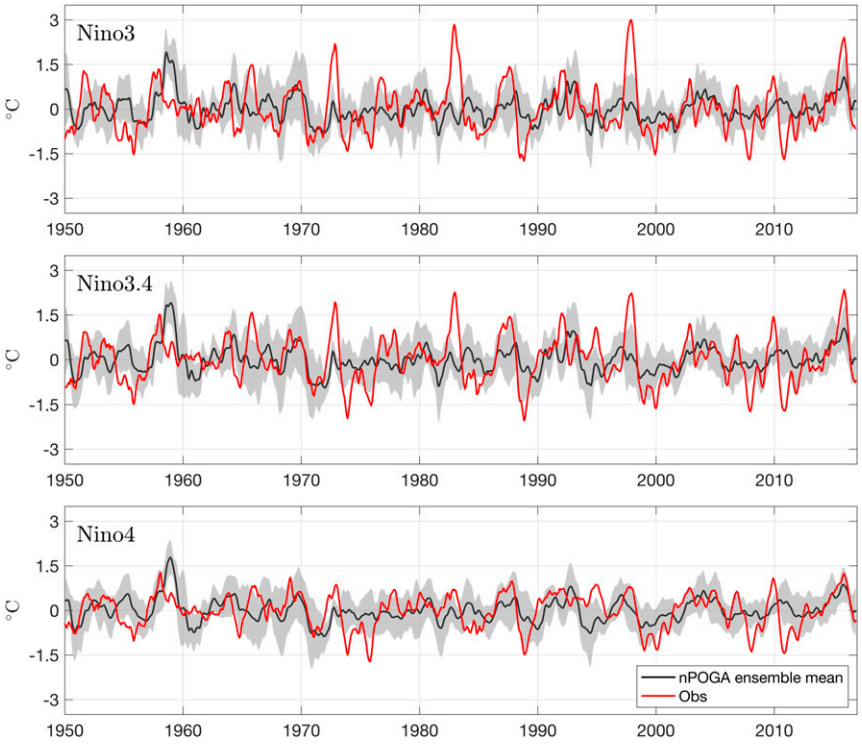

FIG. 2. nPOGA and observed box averaged Niño indices (shown in Fig. 1). Red line in each panel is the observed Niño index and the black line represents the nPOGA ensemble mean simulated Niño index. Shading denotes the 95% confidence ensemble standard error.

Niño-3, Niño-3.4, and Niño-4, respectively). Additionally, the shading indicates that El Niño events in nPOGA tend to be preceded by positive PMM events, while La Niña events tend to be preceded by negative PMM events (R = 0.48, 0.44, and 0.38). Interestingly, the PMM_{CV}/ENSO relationship seems to be more consistent for El Niño events than La Niña events, particularly in Niño-4 where nPOGA La Niña events are not as well simulated compared to observations. Additionally, the nPOGA ENSO events are generally weaker than in observations. This is consistent with a similar analysis conducted by Lu and Liu (2018) and is likely because the nPOGA ENSO values are the ensemble average, and only represent the potential strength of ENSOs forced by the North Pacific.

4. Investigating physical mechanisms in nPOGA

What are the physical mechanisms connecting the North Pacific restoring region in nPOGA to the freely evolving tropical Pacific? Answering this would allow us to better understand why and how nPOGA succeeds at reproducing observed ENSO variability on an event-by-event basis. To begin, we present Hovmöller diagrams that are constructed with nPOGA and nATMO model output and are composited on high ''PMM years'' (see Fig. 6). To highlight the evolution of nPOGA North Pacific SSTs, the Hovmöllers are separated into two pathways (Fig. 5): path A, which stretches northeast-to-southwest from point 0 at 25°N, 122°W to point 6 at 1°N, 178°W, and path B, which runs west-to-east along the equatorial Pacific averaged 3°S–3°N.

Model variables are composited along these paths when the April–June (AMJ) standardized PMM_{CV} is greater than 0.5 standard deviations (N = 19 positive PMM events × 10 ensemble members = 190

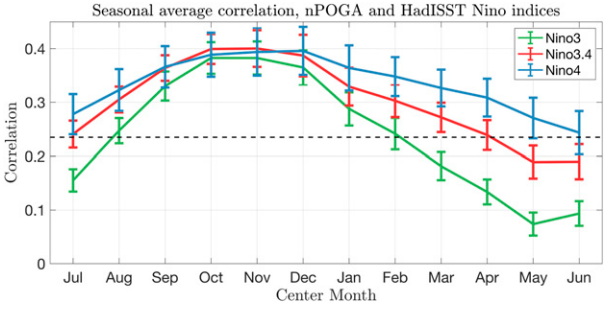

FIG. 3. Seasonal average correlations of nPOGA and HadISST Niño indices. Error bars indicate the 95% confidence ensemble standard error, and the horizontal dashed line indicates a 95% significant correlation after accounting for lag-1 autocorrelation.

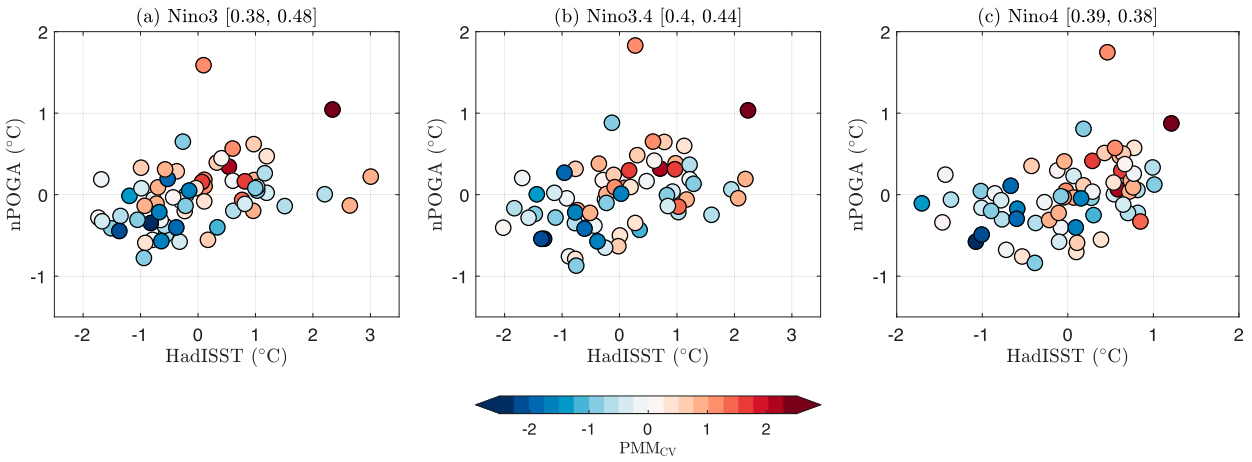

FIG. 4. Scatter of OND Niño indices in HadISST (*x* axis) vs ensemble average of nPOGA (*y* axis). Shading of each circle indicates the magnitude of PMM$_{CV}$ in *preceding* FMA. The first number in each title is the correlation of ensemble mean nPOGA and observed ENSO for that index, and the second number is the correlation of OND nPOGA ENSO with the preceding FMA PMM$_{CV}$. All correlations are significant at the 95% confidence level.

independent samples). When this occurs, it is considered a positive "PMM year" and the data from January of that year (year 0) through April of the following year (year 1) are added to the composite. We choose to composite on AMJ because PMM$_{CV}$ variance is highest in this season (Chiang and Vimont 2004), and we focus on warm PMM events because of the more coherent relationship between nPOGA and observed El Niño events (Fig. 4). Results are insensitive to the choice of compositing season.

a. WES-driven teleconnections to the deep tropics

Figure 6 shows the ensemble mean Hovmöller composites of SSTAs, Q_{LH} anomalies, and zonal 10 m wind (U10) anomalies along paths A and B for nPOGA (left column) and nATMO (right column). Recall that SSTAs in the restoring region (right of vertical black lines) are identical between nPOGA and nATMO. Outside of the restoring region, nPOGA is completely free to evolve and anomalies here are the result of North Pacific SST forcing plus local coupled feedbacks (see data and methods, section 2). Whereas in nATMO, there are no SSTAs outside the restoring region, so atmospheric anomalies here are solely the result of "downstream" North Pacific SST forcing.

Focusing first on the nPOGA Hovmöller composites (Fig. 6; left column), the evolution of SSTAs in the restoring region along path A follow the expected life cycle of a positive PMM event, with warm anomalies peaking in the subtropical North Pacific during boreal spring and largely persisting throughout boreal summer and fall (e.g., Vimont et al. 2009; Alexander et al. 2010). Outside

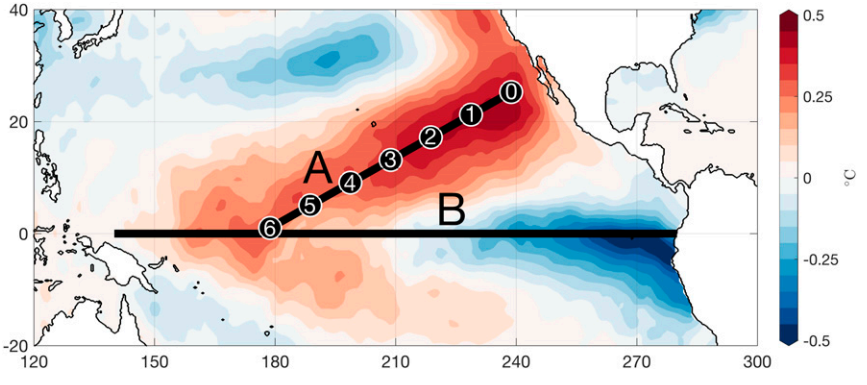

FIG. 5. Schematic illustrating Hovmöller transect paths used for Figs. 6, 7, 11, and 13. Path A follows northeast-to-southwest trajectory from point 0 at 25°N, 122°W to point 6 at 1°N, 178°W. Path B runs west-to-east along the equatorial Pacific Ocean averaged 3°S–3°N. Colored shading represents HadISST SSTAs regressed on the PMM$_{CV}$ index.

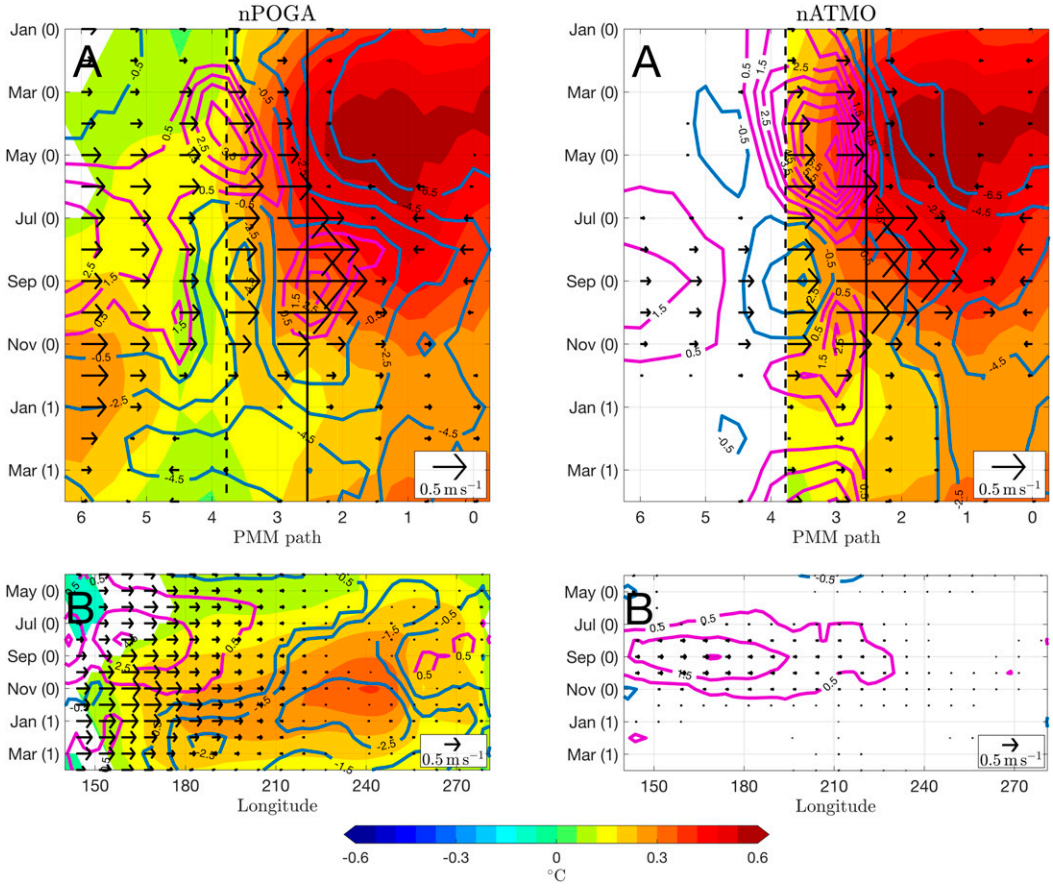

FIG. 6. (left) nPOGA and (right) nATMO ensemble mean Hovmöllers composited on the PMM_{CV} index (see text), and following paths A and B shown in Fig. 5. Shading denotes SSTAs (°C), colored contours indicate latent heat flux anomalies ($W\,m^{-2}$; positive downward), and arrows represent the zonal component of the 10 m wind ($m\,s^{-1}$). The solid black line indicates the edge of the SST restoring region (see section 2), and the dashed black line indicates the edge of the buffer zone. Results are shown only when significant at the 95% confidence level.

of the restoring region where the model is free to evolve, there is a tongue of warm SSTAs that propagates from the edge of the buffer zone in April (0), southwestward along path A, arriving on the equator in July (0). Collocated with these propagating SSTAs are a band of positive Q_{LH} anomalies. These Q_{LH} anomalies are consistent with coincident westerly U10 anomalies that would tend to weaken the background easterly trade winds, reduce evaporative cooling at the surface, and warm the ocean.

The strong spatial continuity, persistence, and southwestward propagation of the SSTAs, Q_{LH} anomalies, and U10 anomalies is consistent with WES feedback theory (Xie and Philander 1994; Amaya et al. 2017), and suggests restoring North Pacific SST in nPOGA excites local air–sea coupled feedbacks that can teleconnect the forced signal into the deep tropics. This conclusion is supported by the nATMO Hovmöller composite (right column), which does not show significant surface wind anomalies outside of the restoring region from January (0) to June (0). The nATMO results do, however, show surface wind and Q_{LH} anomalies within the buffer zone that are larger than nPOGA during this time period, particularly around point 3 of path A. It is possible that the surface winds are stronger due to the reduced SSTA gradient in nPOGA relative to nATMO. Further, nATMO Q_{LH} anomalies are likely larger because there is not an interactive ocean to dampen these fluxes (Barsugli and Battisti 1998). In contrast, the nPOGA ocean model becomes increasingly interactive within the buffer zone moving equatorward of 15°N, which would tend to dampen fluxes there. Additionally, while changes in low cloud fraction have also been shown to contribute to the evolution of subtropical North Pacific SSTAs through a modification of downwelling surface shortwave radiation (e.g., Vimont et al. 2009), we do not find evidence that increased shortwave anomalies are required to drive these propagating SSTAs in nPOGA. Instead, positive downwelling shortwave anomalies only

act to reinforce the warm SSTAs within the restoring region (not shown).

Once the WES-driven SSTAs and U10 anomalies arrive on the equator, they grow in magnitude and persist into the following year (Fig. 6, left column, path A), suggesting the presence of additional local feedbacks that act to amplify the signal. The downward latent heat flux anomalies from July (0) to November (0) in path A of both the nPOGA and nATMO simulations indicate a potential role for WES feedback to continue amplifying the western equatorial Pacific SSTs (note that in the nPOGA simulation these downward flux anomalies occur over positive SSTAs, indicating an important role for wind speed variations). At the same time, the westerly wind anomalies can excite dynamical feedbacks that amplify SST across the basin.

Further evidence of this can be seen in nPOGA path B. This east–west Hovmöller plot shows warm, El Niño–like SSTAs beginning to grow during May (0) in the eastern equatorial Pacific, while significant westerly wind anomalies persist in the western equatorial Pacific. The position of the warm SSTAs in the east relative to the remote wind forcing in the west suggests the importance of ocean dynamics (e.g., downwelling Kelvin waves) in maintaining the warm SSTAs on the equator. From June (0) to March (1), the SSTA maximum strengthens and spreads from east to west as the U10 anomalies also grow in the west and central equatorial Pacific, both ultimately peaking in November (0). These results suggest that North Pacific SSTAs alone, through a WES-driven teleconnection, are sufficient to drive equatorial westerly wind anomalies that can initiate Bjerknes feedbacks and generate an El Niño event in the model.

b. *Mean state interactions and "downstream" forcing of tropical winds*

Interestingly, the nATMO Hovmöller diagrams (Fig. 6, right column) also show significant surface wind anomalies from July (0) to November (0) extending from the restoring region in the subtropical North Pacific (path A) all the way to the equator (path B). This suggests that a component of the equatorial westerly wind anomalies in nPOGA is a direct response to the restored North Pacific SSTs. To investigate this relationship further, we compare the nATMO SSTAs and U10 anomalies from Fig. 6 with nATMO precipitation anomalies (mm day^{-1}; colored contours) composited along path A (Fig. 7). For reference, we also plot the position of the climatological ITCZ (gray shading) by showing precipitation averaged in the Pacific 150°E–100°W at each latitude indicated by the upper x axis.

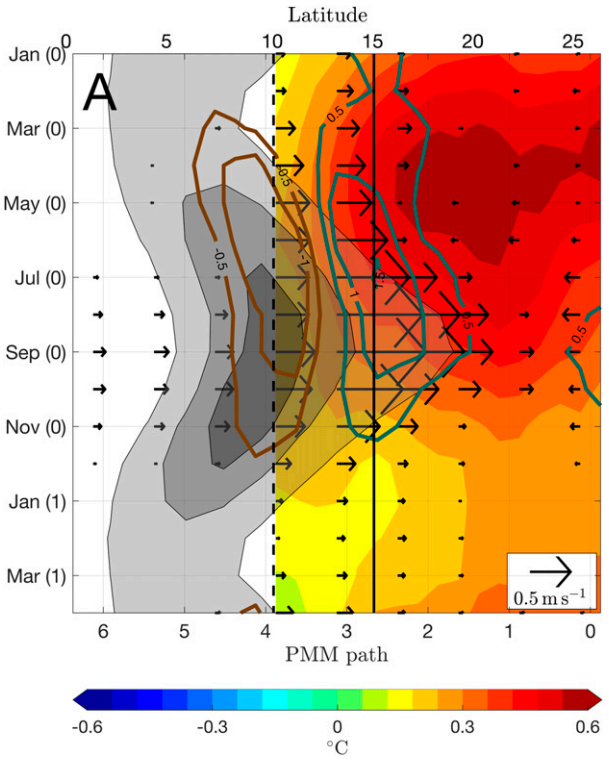

FIG. 7. As in Fig. 6 (top right), but the colored contours are now precipitation anomalies (mm day^{-1}). Gray shading denotes the climatological precipitation averaged in the Pacific 150°E–100°W (4, 8, and 12 mm day^{-1} from the light to heavy shading, respectively), representing the ITCZ. Note this gray shading follows the latitudinal lines indicated by the upper x axis and is not averaged along path A.

Figure 7 shows a dipole of precipitation anomalies persisting from March (0) to November (0), with increased precipitation over the warm SSTAs in the restoring region, and decreased precipitation along the edge of the buffer zone. This precipitation pattern is consistent with anomalous convection driven by increased surface wind convergence over the warm SSTAs and would tend to produce an anomalous northward shift of the climatological ITCZ. Though the precipitation anomalies persist in time along with the warmest SSTAs, the U10 anomalies do not significantly extend toward the equator until late boreal summer into boreal fall. This can be explained by the timing of the warmest subtropical SSTAs relative to the position of the mean ITCZ during its seasonal migration. In boreal spring, when the PMM peaks, the ITCZ is closest to the equator and is less sensitive to off-equatorial SSTAs. In contrast, during the late summer and fall, the ITCZ is farthest north and is more easily influenced by the persistent warm conditions in the subtropical North Pacific.

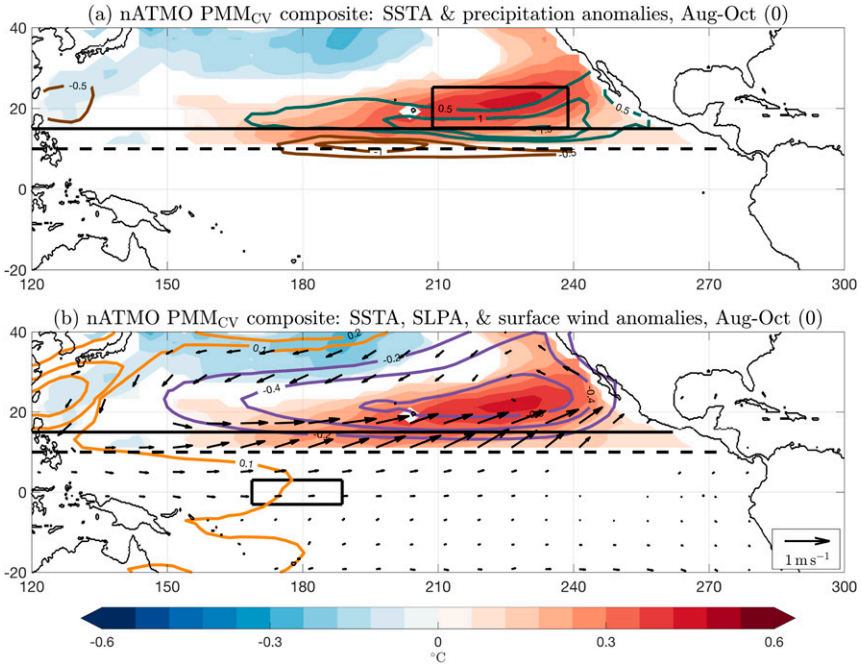

FIG. 8. (a) nATMO ensemble mean SSTA (°C; shading) and precipitation anomalies (mm day^{-1}; colored contours) composited on same PMM$_{CV}$ events as Fig. 6, but for August–October (0). (b) Same SSTAs as in (a), overlaid with SLPA (hPa; colored contours) and 10 m wind anomalies (m s^{-1}). Solid and shaded black horizontal lines denote the edge of the SST restoring region and buffer zone, respectively. Black boxes in (a) and (b) refer to calculations made for Fig. 9 (see text).

This atmospheric response can be seen clearly in the horizontal view of nATMO August–October (ASO) composited SSTAs, precipitation anomalies, sea level pressure anomalies (SLPAs), and surface wind anomalies (Fig. 8). In Fig. 8a, the largest precipitation response is from 180° to the Mexican coastline. The atmospheric circulation induced by the associated convective heating is generally consistent with the tropical atmospheric response to an off-equatorial heat source (e.g., Gill 1980), which produces the significant surface winds seen in Fig. 6 (right column). Figure 9 further illustrates the importance of the late summertime subtropical SSTAs to this equatorial wind response by comparing ASO SSTAs averaged from 15°–25°N, 150°–120°W (black box, Fig. 8a) to a westerly wind index (U_{eq}) computed by averaging nATMO zonal wind anomalies from 3°S to 3°N, 170°E to 170°W (black box, Fig. 8b). Consistent with the composite analysis, we find that the nATMO U_{eq} index is significantly correlated with the prescribed subtropical SSTAs ($R = 0.68$).

While Figs. 7–9 illustrate the strong seasonality of the uncoupled response, we note that Vimont et al. (2009) report a similar seasonality using coupled simulations. Further, Vimont et al. (2009) indicate that ocean–atmosphere coupling tends to amplify the downstream U10 response and can drive it even closer to the equator during late boreal summer and boreal fall.

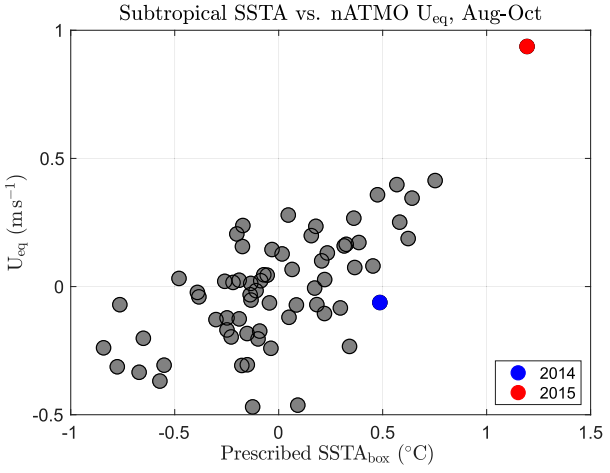

FIG. 9. Scatter of SSTA (°C) used to force nATMO, averaged in the subtropical black box in Fig. 8a (x axis), vs nATMO ensemble mean zonal wind anomalies (m s^{-1}) averaged in the equatorial black box in Fig. 8b (y axis). Blue and red dots represent values for 2014 and 2015, respectively.

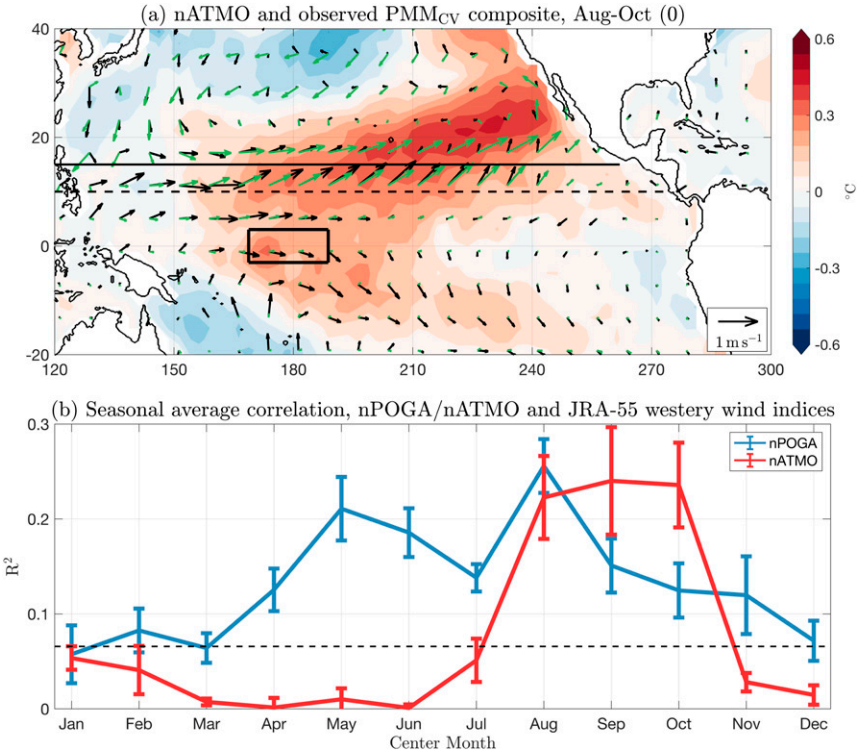

FIG. 10. (a) Observed SSTA (°C; shading) and 10 m wind anomalies (m s^{-1}; black arrows) composited on same PMM$_{CV}$ events as in Fig. 6, but for August–October (0). Green arrows are nATMO ensemble mean winds for the same composite period. (b) Seasonal R^2 value between JRA-55 U10 anomalies and nPOGA (blue) and nATMO (red) averaged in the equatorial black box in (a). Error bars indicate the 95% confidence ensemble standard error, and the horizontal dashed line indicates a 95% significant R^2 value after accounting for lag-1 autocorrelation.

c. *Quantifying the "summer deep convection" response in observations*

The analysis of nATMO in Figs. 6–9 highlights the striking interaction between the mean ITCZ and warm subtropical SSTAs that are related to the persistence of the PMM into boreal summer. This interaction provides a second pathway for the North Pacific to re-energize WES feedback, remotely influence the deep tropics, and interact with ENSO. For clarity, we introduce the term "summer deep convection" (SDC) response to refer to this additional teleconnective pathway. The SDC response as seen in Fig. 8 is reminiscent of results outlined by Vimont et al. (2001) and others, who focused on the overall evolution of the SFM by analyzing the impact of summertime subtropical SSTs on the tropical atmosphere. Indeed, Fig. 4b in Vimont et al. (2001) compares well with Fig. 8 of this study. Given that nATMO is forced by observations, we can utilize our simulations to cleanly isolate the impact of the SDC response on historical equatorial surface winds. Equatorial winds around the date line are routinely used as an indicator and predictor of ENSO conditions. Thus, such an analysis could potentially improve ENSO predictability on seasonal time scales.

Figure 10a shows ASO averaged HadISST SSTAs (shading) and JRA-55 10 m wind anomalies (black arrows) composited on the same AMJ PMM$_{CV}$ events as in Figs. 6–8. Overlaid in green arrows are ensemble mean nATMO composite wind anomalies in ASO. Since nATMO is forced by observed SSTAs north of 15°N, we can compare the magnitude and direction of the observed (black) and simulated (green) winds to gain some intuition for how the observed wind field is impacted by the SDC-forced wind anomalies.

In both observations and nATMO, there is a basin-wide anomalous cyclonic circulation centered around 20°N that is associated with the thermally driven low pressure center. There are slight differences in wind magnitude in the restoring region, which may be due to the difference in sample size between the nATMO and observed composites (190 vs 19 samples, respectively). Nevertheless, the close overall agreement between the two wind fields suggests the observed wind structure is largely a direct response to the underlying SSTAs. South

of the restoring region, the magnitude of the nATMO winds decreases relative to observations due to the absence of amplifying effects from coupled feedbacks. However, along the equator, the nATMO winds continue to show some skill in simulating the observed winds, particularly around the date line, indicating that the SDC response may significantly contribute to the time variability of observed westerly winds in this region.

To quantify the equatorial westerly wind variance explained by North Pacific SSTAs in observations, we create a westerly wind index by averaging 10 m zonal wind anomalies from 3°S to 3°N, 170°E to 170°W (black box, Fig. 10a). We then correlate seasonally averaged values of this index between nATMO and JRA-55 from 1958 to 2016. This process is repeated with nPOGA for comparison, and the results are shown in Fig. 10b. nATMO only produces a significant correlation with observations in late boreal summer and early boreal fall, which is consistent with our hypothesis that subtropical North Pacific SSTAs are most effective at remotely influencing the deep tropics when the mean ITCZ is farthest north (Fig. 7). Based on this calculation, about 25% of the observed time variability of August–October equatorial U10 anomalies can be explained by the remote SDC response in the North Pacific.

In comparison, nPOGA explains significant portions of the observed U10 index through much of the year, with separate peaks in May and August. This first peak explains 20% of the variance and can be interpreted as the contribution to the observed equatorial U10 variance by surface winds forced by local air–sea interactions such as WES feedback. The second peak explains about 25% of the variance and is likely also due to the SDC response. The decrease in correlation after the August peak may be due to other ocean–atmosphere interactions, which are present in nPOGA and not nATMO. This would add additional noise to nPOGA that may lower the overall correlation. This highlights the difficulty of separating the nPOGA wind contribution due to mixed layer coupled feedbacks (e.g., WES feedback) relative to coupled feedbacks involving a dynamical ocean (e.g., Bjerknes feedback). Ideally, additional comparisons would be made to an atmospheric model coupled to a mixed layer ocean, but that is beyond the scope of this study. We encourage future modeling efforts on this topic.

5. The 2014–16 ENSO cycle, a case study

We showed that in nPOGA, ENSO events can be initiated by local air–sea interactions (i.e., WES feedback and Bjerknes feedback) excited by restored North Pacific SSTAs. These tropical signals can also be amplified and/or reinforced in boreal summer by locally uncoupled surface winds generated by the subtropical SDC response. In the real world, the efficacy of these different teleconnections to influence the development of an ENSO event would depend on the internal state of the tropics when the North Pacific signal ''arrives.'' This signal-to-noise problem is further highlighted by the large spread in Niño indices among nPOGA ensemble members, which makes an event-by-event comparison between the model and observations difficult (Fig. 2).

However, nPOGA does show remarkable reproducibility of several ENSO events, including the weak 2014/15 El Niño and the extreme 2015/16 El Niño. Given the broad scientific interest in these two El Niños (e.g., Hu and Fedorov 2016; Maeda et al. 2016; Levine and McPhaden 2016; Hu and Fedorov 2019; Siler et al. 2017), a more in-depth comparison between nPOGA, nATMO, and observations during this time period is appropriate. In this section we will take advantage of the physical intuition developed in section 4 to analyze the 2014–16 ENSO cycle as a case study.

a. The weak 2014/15 El Niño

Figure 11 shows similar Hovmöller diagrams to Fig. 6, but for the weak 2014/15 El Niño event in observations (left column) and the ensemble means of nPOGA (middle column) and nATMO (right column). Note the different wind scales. Focusing first on observed path B, we see significant westerly U10 anomalies centered around 160°E from January to May 2014. These westerly wind events drove a series of downwelling Kelvin waves that suppressed upwelling and lead to warm SSTAs in the eastern equatorial Pacific beginning in May 2014. The strength of these wind events in conjunction with the magnitude of the eastern equatorial SSTAs and subsurface thermocline anomalies led many in the scientific community to believe a strong El Niño was developing (Pacific ENSO update, 2014).

However, a series of easterly wind events in the western equatorial Pacific during summer 2014 stunted the development of the El Niño by suppressing the positive Bjerknes feedback critical to its growth (Hu and Fedorov 2016). JRA-55 does not show easterly wind anomalies during this time period, but there is a pronounced weakening of the westerly wind anomalies in June–July 2014 (Fig. 11, left column, path B). As a result, the developing 2014 El Niño weakens substantially, and never quite recovers. Instead, the observed SSTAs remain fragmented around the central Pacific, and the U10 anomalies in the west Pacific do not amplify, suggesting Bjerknes feedback does not fully establish.

Comparing to the nPOGA ensemble mean (Fig. 11, left and middle columns, path B), we find the pacemaker

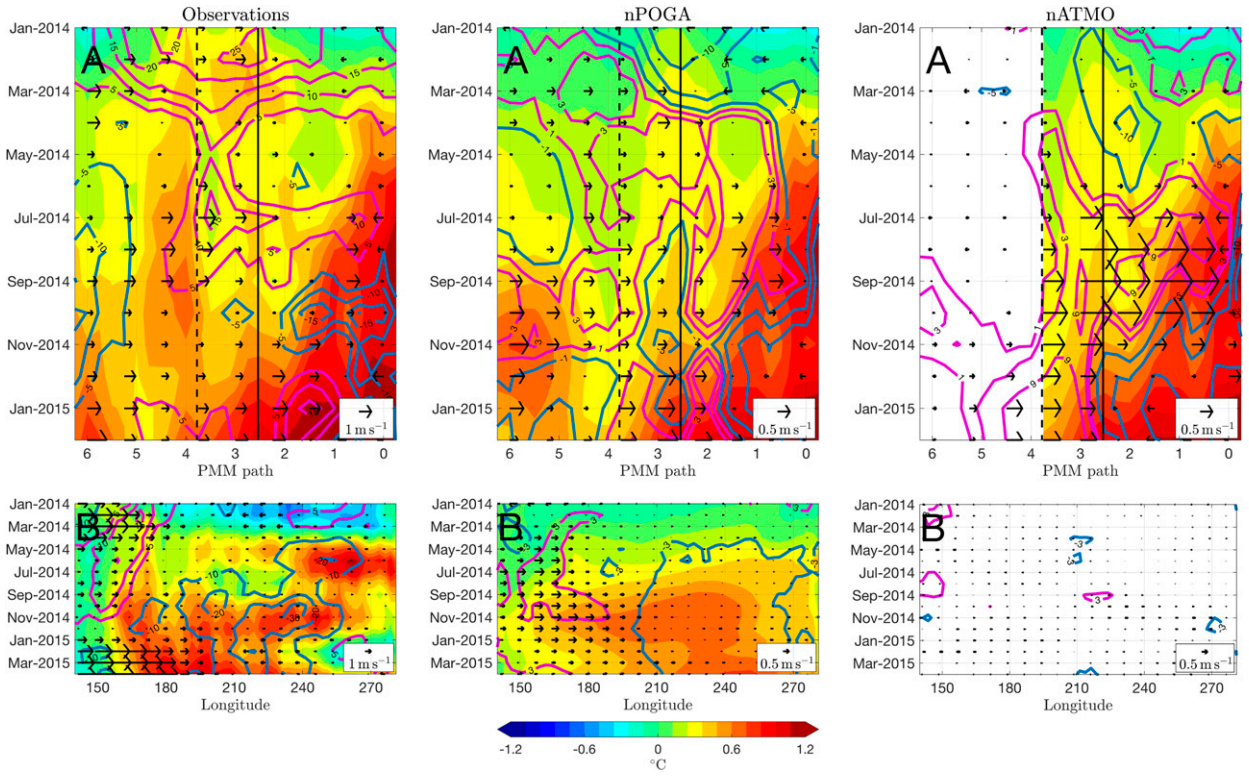

FIG. 11. As in Fig. 6, but Hovmöllers across the 2014/15 El Niño event in (left) observations, (middle) nPOGA ensemble mean, and (right) nATMO ensemble mean. For clarity, nPOGA and nATMO winds are scaled by 2 relative to observations.

experiment does a remarkable job of simulating the overall timing and magnitude of the main 2014 El Niño. However, the initial westerly wind anomalies observed in winter/spring 2014 and the first observed SSTA maxima in boreal summer are not seen in nPOGA, suggesting that in reality they were the result of processes independent of the North Pacific. Following these events, nPOGA features a series of consistent westerly U10 anomalies west of 180° from April–August 2014 which give rise to an El Niño event that evolves more smoothly than observations.

The general consistency between the nPOGA and observed equatorial SST and wind anomalies during this time period suggests the real-world evolution of the 2014 El Niño was influenced by the North Pacific. This connection can be further diagnosed by comparing Fig. 11 (path A) to the composites presented in Fig. 6. In each upper panel of Fig. 11, the SSTAs depict a moderate positive PMM event evolving from spring 2014 to winter 2015. The time evolution of SSTAs in the restoring region is not as coherent as the canonical PMM event seen in Fig. 6, even showing a temperature increase throughout the year instead of dampening as in the composite. The different SSTA evolution may be expected, as 2014 represents a single PMM event, and therefore provides an indication of the diversity present among all events.

Despite these differences, Fig. 11 shows a general southwestward propagation of SSTAs in observations (path A, left column) and in nPOGA (path A, middle column), suggesting the presence of similar coupled processes to the composite. We indeed see evidence of WES feedback via a band of positive Q_{LH} anomalies and collocated westerly U10 anomalies extending from the restoring region southwestward toward the equator from boreal spring to summer. In observations, there is a similar, albeit less coherent, propagating band of Q_{LH} and U10 anomalies from May–September 2014. nATMO (Fig. 11, path A, right column) fails to reproduce these winds, further supporting the role of local air–sea coupling in nPOGA and observations. Interestingly, we also note nATMO does not show a clear SDC response during summer 2014. This is peculiar given the strength of the warm SSTAs used to force the model (Fig. 9). We will discuss this in more detail in section 5c.

To analyze the influence of the North Pacific on the weak 2014/15 El Niño event, we also compare horizontal plots of SSTAs, Q_{LH}, and surface wind anomalies (Figs. 12a–d). In FMA 2014, the warm PMM SSTAs are completely enveloped by positive Q_{LH} anomalies,

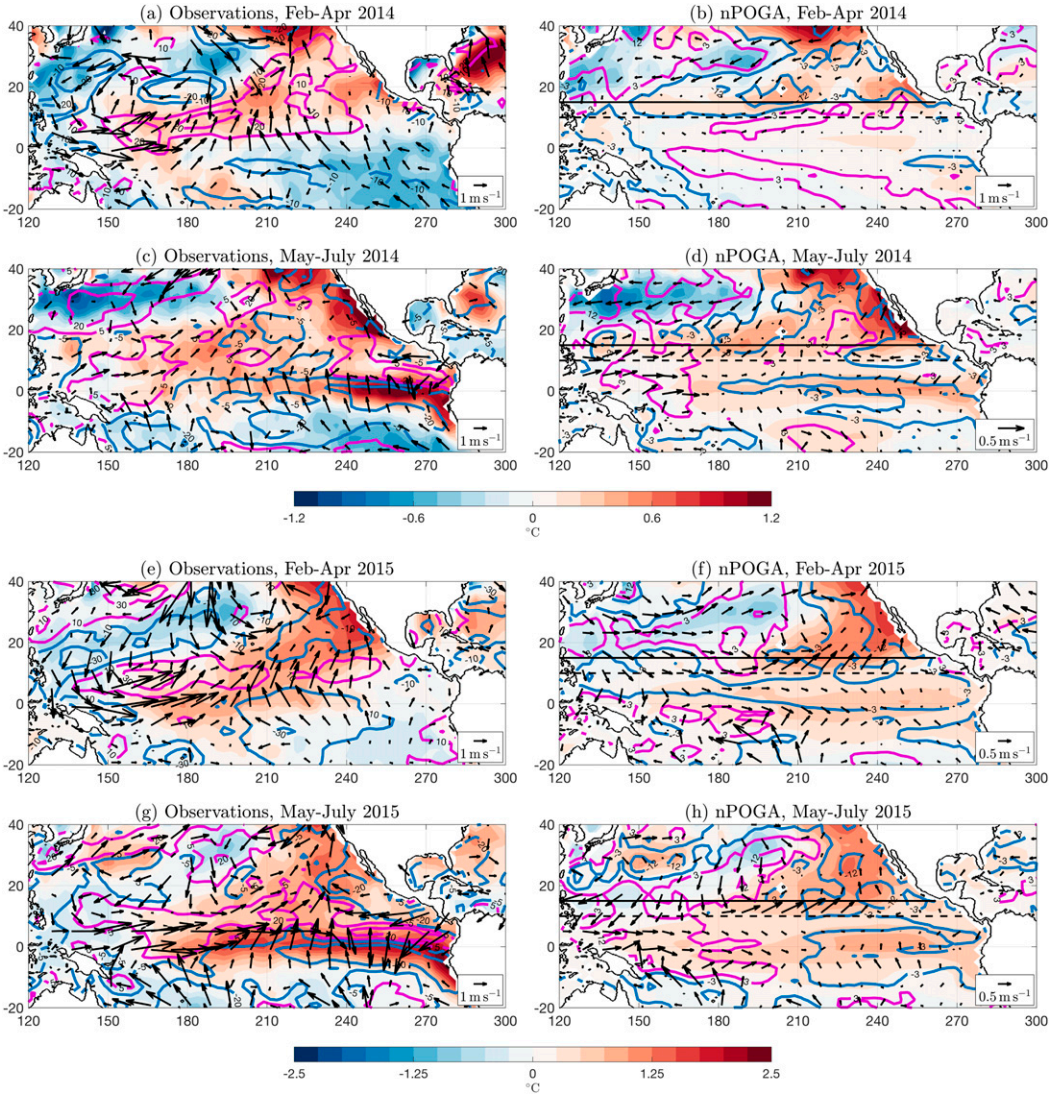

FIG. 12. In all panels shading is SSTAs (°C), black arrows are 10 m wind anomalies (m s^{-1}), and colored contours are latent heat flux anomalies (W m^{-2}; positive downward). (a),(c) Observations averaged for February–April 2014 and May–July 2014, respectively. (b),(d) nPOGA ensemble mean values averaged over the same seasons. (e)–(h) As in (a)–(d), but for 2015. For clarity, nPOGA winds are scaled by 2 relative to observations.

suggesting that the ocean has not yet forced an atmospheric response (Vimont et al. 2003a). In May–July (MJJ) 2014 (Fig. 12c), observations show a tilted dipole of Q_{LH} anomalies, with positive anomalies around 0°–20°N, 140°E–180° and negative anomalies to the northeast around 10°–25°N, 190°–220°W. Collocated with the positive Q_{LH} anomalies are surface southwesterly anomalies extending south from 20°N. In combination with the surface wind anomalies, the MJJ Q_{LH} dipole further supports the hypothesis that WES feedback was active in observations (Amaya et al. 2017), ultimately forming westerly winds on the equator in FMA and MJJ 2014.

Figures 12b and 12d depict the evolution of nPOGA during the same time periods. Note the different wind scales. In response to the restored SSTAs, nPOGA produces surface southwesterly anomalies converging in the subtropics near the edge of the buffer zone. In MJJ, there is a tilted Q_{LH} dipole with positive Q_{LH} and southwesterly anomalies from 0° to 10°, 140° to 170°E that are very similar to observations (Figs. 12c,d). As such, nPOGA features comparable equatorial wind anomalies in the west Pacific that are favorable for the development of an El Niño in the model.

There are, however, some notable differences between nPOGA and observations. For example,

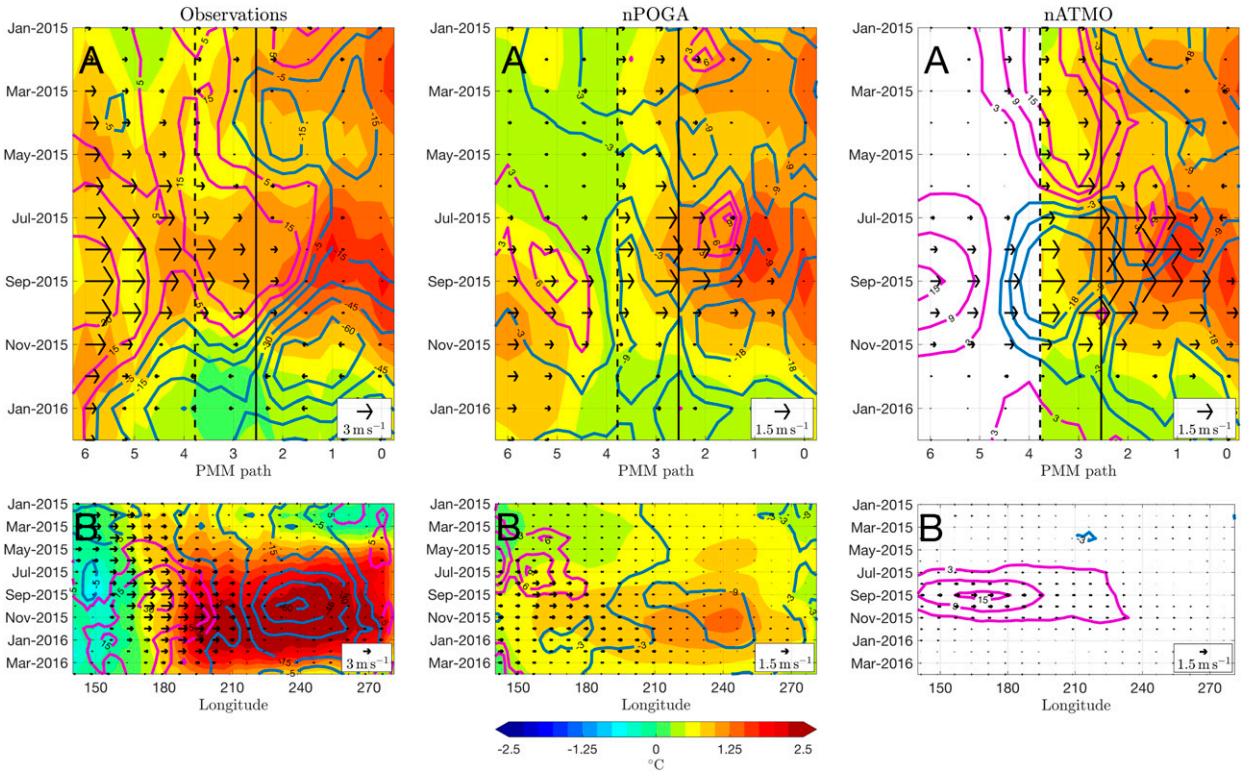

FIG. 13. As in Fig. 11, but for the 2015/16 El Niño event in (left) observations, (middle) nPOGA ensemble mean, and (right) nATMO ensemble mean. For clarity, nPOGA and nATMO winds are scaled by 2 relative to observations.

observations show persistent southeasterly surface wind anomalies in the eastern equatorial and southeast tropical Pacific that are collocated with cool SSTAs. These signals are not reproduced in nPOGA, suggesting that they are independent of North Pacific forcing. The observed southeasterly surface wind anomalies in the eastern Pacific may instead be related to a long-term trend in cross-equatorial flow driven by multidecadal cooling in the southeastern Pacific (e.g., Amaya et al. 2015) and/or warming in the tropical Atlantic (Hu and Fedorov 2018).

Despite these differences, the combined results of Figs. 11 and 12a–d lead us to conclude that late boreal spring to early boreal summer equatorial wind forcing associated with the 2014/15 El Niño was significantly impacted by North Pacific SSTAs through the WES feedback propagating mechanism outlined in section 4. Further, the smooth, unbroken evolution of these equatorial winds in nPOGA suggests that the North Pacific forcing may have generated a more consistent 2014/15 El Niño event if not for tropical internal variations.

b. *The extreme 2015/16 El Niño*

Figure 13 shows the same Hovmöller transects as in Fig. 11, but for the extreme 2015/16 El Niño event. Note the change in color bar and wind scale. In early 2015, the remnants of the 2014/15 El Niño can be seen as a zonal dipole of positive SSTAs in the central equatorial Pacific and neutral SSTAs in the eastern equatorial Pacific (Fig. 13, left column, path B). A series of westerly wind events in the western Pacific from January–May 2015 then act to drive downwelling Kelvin waves, thereby warming eastern Pacific SSTAs and amplifying the zonal wind response along the equator. Throughout the rest of the year, the SSTAs grow in amplitude, culminating in one of the warmest El Niño events on record.

Concurrently, the observed path A shows the evolution of the strongest positive PMM event in at least the last 70 years, as indicated by the red circle in Fig. 9. During this event, the warm SSTAs propagate along with a band of positive Q_{LH} and westerly anomalies southwestward from the subtropics in March 2015 to the equator around July 2015, indicating a positive WES feedback. This result is further supported by Fig. 12e, which shows the telltale dipole of Q_{LH} anomalies, collocated southwesterly U10 anomalies, and cross-equatorial flow in FMA 2015. By MJJ, wind-driven ocean dynamics produce a developing El Niño response in the eastern equatorial Pacific (Fig. 12g).

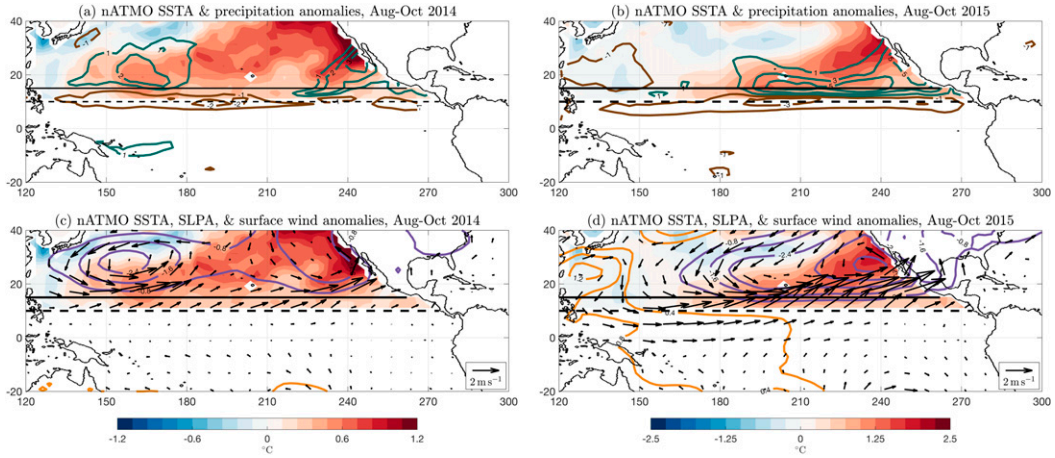

FIG. 14. As in Fig. 8, but for (a),(c) August–October 2014 and (b),(d) August–October 2015.

The nPOGA ensemble mean captures many of these features, producing an El Niño event that peaks in November–January 2015/16 and results from a band of westerly wind events beginning in April 2015 (Fig. 13, middle column, path B). However, the WES feedback response is less clear in the model. Instead, the restored SSTAs appear disconnected and unrelated to the tropical anomalies (Fig. 13, middle column, path A). The reason for this discrepancy may be due, in part, to the different evolutions of the 2014/15 El Niño event in observations and the nPOGA ensemble mean. In reality, the developing 2014 El Niño faltered, and ultimately failed to initiate a significant Bjerknes response, which left the equatorial Pacific in a CP El Niño–like state in the early parts of 2015 (Fig. 12e). In contrast, without the interference of internal tropical variations, the nPOGA ensemble mean shows a 2014 El Niño that persists into 2015. These lingering warm anomalies appear to drive an anomalous surface wind convergence along the eastern equatorial Pacific (Fig. 12f), preventing efficient WES feedback interactions outside the restoring region. Whereas in observations, the more neutral eastern equatorial Pacific leaves the tropical atmosphere more sensitive to subtropical SSTA forcing.

By running an ensemble of nPOGA experiments, we have sampled a range of possible internal tropical states with which the restored North Pacific SSTAs may interact. As a result, there is a small subset of ensemble members whose 2014/15 El Niño declines in a similar manner to observations. In these runs, the absence of warm eastern equatorial waters allows the tropical surface winds to more directly respond to the subtropical SST forcing, producing a more consistent WES feedback (not shown). This result and the results of Figs. 12e and 12f support our interpretation above and suggest a more detailed investigation into the interaction between North Pacific teleconnections and different internal tropical states is warranted. Such an analysis is outside the scope of the current work, but we do plan to thoroughly investigate the nPOGA ensemble spread in a future study.

Our analysis of the observations in Figs. 12 and 13 suggests WES feedback contributed to the early development of the observed 2015/16 El Niño. There is also evidence that the equatorial wind forcing was amplified in summer 2015 by a significant SDC response. This is indicated by the nATMO ensemble mean winds, which extend from the subtropics to the equator in Fig. 13 (right column). Figures 14b and 14d show the nATMO ensemble mean atmospheric response for ASO 2015. The northward shifted ITCZ, the zonal SLPA dipole in the subtropics, and the significant westerly surface wind anomalies on the equator are all very similar to the composite structures seen in Fig. 8. By averaging zonal wind anomalies around the date line (Fig. 8b, black box) in observations and nATMO, we calculate that the SDC effect increased the strength of surface winds along the equator by 20% in ASO 2015, potentially contributing the extreme nature of the 2015/16 El Niño.

c. Differences in the 2014 and the 2015 SDC responses

The importance of the SDC response to the development of the 2015/16 El Niño event stands in stark contrast to the 2014/15 El Niño event, which did not produce significant equatorial winds in nATMO (Fig. 11, right column). This is peculiar given the strength of the subtropical SSTAs in ASO 2014, which are among the warmest since 1950 (Fig. 9). To investigate the source of the different atmospheric responses, Fig. 14 shows the nATMO precipitation anomalies, surface wind anomalies, SLPAs, and SSTAs for ASO 2014 (Figs. 14a,c) and ASO

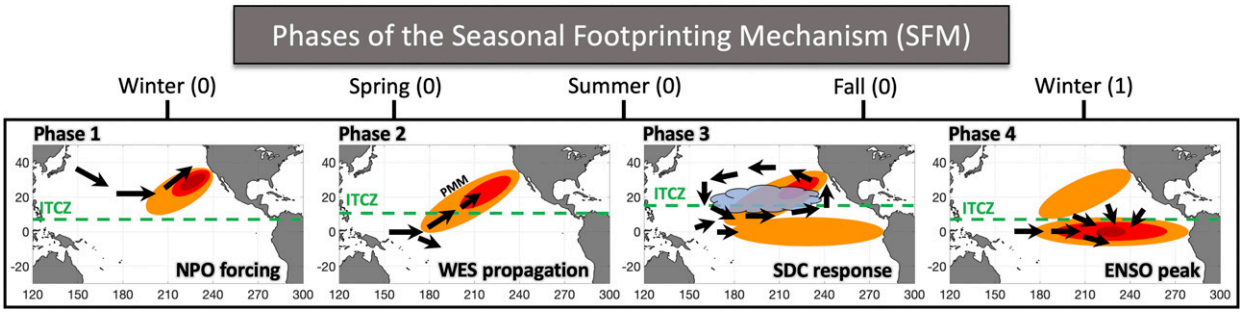

FIG. 15. Schematic summarizing the phases of the seasonal footprinting mechanism (SFM) as described in this study. Colored shading denotes SSTAs. Black arrows are surface wind anomalies. Dashed green line is approximate position of the mean ITCZ. Shaded cloud represents anomalous precipitation. Upper axis depicts approximate timing of phases from winter of year 0 to winter of year 1. Phases are as follows: Phase 1: NPO-forced modulation of trade wind strength leaves SST "footprint" through anomalous latent heat flux. Phase 2: Footprint SSTAs reinforced by mixed layer feedbacks. Surface anomalies teleconnected to the deep tropics for the first time via PMM WES propagation mechanism, creating ENSO-favorable equatorial winds. Phase 3: Mean ITCZ at northerly most extent and sensitive to persistent PMM SSTAs. Surface anomalies teleconnected to the deep tropics for the second time via SDC response. WES feedback and ENSO conditions are reinforced. Phase 4: Subtropical anomalies dampen, Bjerknes feedback takes hold, and ENSO reaches its peak.

2015 (Figs. 14b,d). Note the different color bars and precipitation contour intervals.

Compared to 2015, the warm SSTAs in 2014 are generally weaker and extend farther northward and westward. In ASO 2014, the main convective response has been broken up into two distinct maxima in the western and eastern North Pacific, which results in fragmented circulation anomalies (Figs. 14a,c). In contrast, the precipitation peak in ASO 2015 is spread more uniformly throughout the eastern North Pacific. As a result, the convective center in ASO 2015 generates a broad and coherent cyclonic circulation (Figs. 14b,d) that compares well with the earlier composites (Fig. 8).

These different equatorial wind responses may be due to the horizontal displacement of the warmest SSTAs in 2014 relative to 2015, which could account for the circulation differences in the subtropics and the extent to which they project along the equator. Another possibility could be that the subtropical SSTAs in 2014 were simply too weak to generate a coherent shift in the ITCZ. However, Fig. 9 shows that there are years with comparably warm subtropical SSTAs that produce a more significant equatorial wind response. Regardless of precise mechanisms, Figs. 9 and 14 illustrate the potential importance of the strength and pattern of subtropical SSTAs to the summertime tropical atmospheric response. Targeted modeling experiments are needed to determine the sensitivity of the tropical atmosphere to different regional subtropical SSTA perturbations.

6. Summary and discussion

In this study, we have presented the first North Pacific pacemaker experiment designed to investigate the connection between the North Pacific and ENSO in the historical record. We found that teleconnections driven by North Pacific SSTAs can account for a significant fraction of observed ENSO variability since 1950, especially in boreal fall and winter. These teleconnections (as summarized in Fig. 15) are made possible, in part, by an interaction between SSTAs, latent heat flux anomalies, and surface wind anomalies known as WES feedback (Xie and Philander 1994; Amaya et al. 2017), which propagates the restored North Pacific forcing into the deep tropics during boreal spring and summer (phase 2, Fig. 15).

We also compared our nPOGA results to an ensemble of atmosphere-only runs, and identified an important secondary pathway for the North Pacific to influence tropical ocean–atmosphere variability during late boreal summer and fall. This second teleconnection is related to earlier work that focused on the evolution of the SFM (e.g., Vimont et al. 2001, 2003a,b), and stems from an interaction between North Pacific SSTAs and the mean position of the ITCZ during its seasonal migration. During the late summer, persistent PMM-related SSTAs force an anomalous northward shift of the ITCZ, which results in thermally driven circulation anomalies that resemble the atmospheric response to an off-equatorial heat source (Gill 1980). This process, which we refer to as the summer deep convection (SDC) response, produces significant surface winds along the equator that can influence equatorial SSTAs and ENSO through WES feedback and ocean dynamics (phase 3, Fig. 15). We showed that the SDC response accounts for about 25% of the observed equatorial zonal wind time variability during late boreal summer and early boreal fall.

The nPOGA simulation's overall skill is generally consistent with a recent study by Lu and Liu (2018), which assessed the extratropical impact on historical ENSO by assimilating observed ocean and atmosphere data at varying latitudes in a fully coupled spectral model. In particular, the correlations between nPOGA-simulated ENSO and observations are comparable to those reported by Lu and Liu (2018) when they assimilated only ocean data poleward of 10° or 15°. Despite these similarities, our work is more targeted at quantifying the physical mechanisms that connect the North Pacific to the tropics. This is different from Lu and Liu (2018), who assimilate data in both hemispheres simultaneously and at all longitudes.

Building on the physical intuition laid out in section 4, we then analyzed the weak 2014/15 El Niño and the extreme 2015/16 El Niño as case studies in nPOGA. Our results suggested that the development of the 2014/15 El Niño was aided by a positive WES feedback teleconnection from the North Pacific, which drove significant westerly winds on the equator and generated an El Niño in the model. This confirms earlier speculation by Di Lorenzo and Mantua (2016), who hypothesized that the 2013–15 North Pacific marine heat wave (Bond et al. 2015; Amaya et al. 2016) may have included a positive PMM event that contributed to the development of the 2014/15 El Niño. Our study suggested these interactions did occur in reality; however, internal tropical variations severely limited the effectiveness of 2014 PMM in creating a smoothly evolving 2014/15 El Niño (Hu and Fedorov 2016).

The extreme 2015/16 El Niño was preceded by the warmest subtropical North Pacific SSTAs in at least the last 70 years (Fig. 9, red circle). We presented observational evidence that these 2015 SSTAs generated a positive WES feedback, which propagated the North Pacific surface anomalies into the deep tropics where they could influence equatorial ocean dynamics. In addition to WES feedback, we showed that North Pacific SSTAs triggered a robust SDC response during boreal fall 2015. As a result, the large-scale circulation anomalies drove surface wind anomalies along the equatorial Pacific and enhanced ocean forcing by 20% during this time period, potentially contributing to the extreme nature of the 2015/16 El Niño.

By providing observational context, our analysis has highlighted several key points that should be considered in future research. First, we echo previous studies pointing to the impact of the tropical internal state on the efficacy of North Pacific teleconnections (e.g., Vimont et al. 2009; Alexander et al. 2010; Park et al. 2013). The atmospheric response to North Pacific SSTAs is small relative to similar perturbations in the tropics. Thus, the effectiveness of North Pacific teleconnections is heavily modulated by the timing of the signal's "arrival" relative to the timing of tropical noise, which can include atmospheric modulations across the tropics such as the Madden–Julian oscillation (Kim et al. 2018) and the buildup or recent discharge of ocean heat content in the west Pacific upper ocean (Jin 1997).

Second, nPOGA focuses on North Pacific teleconnections; however, the South Pacific has also been shown to be an important source of equatorial Pacific variability (Zhang et al. 2014a; Lu et al. 2017; You and Furtado 2017; Larson et al. 2018). A more detailed analysis of observed South Pacific teleconnections and how they interact with signals from the North Pacific would improve our understanding of ENSO. As a result, we plan to analyze a South Pacific pacemaker experiment in a future study.

Finally, while our experimental design addresses many of the limitations found in previous studies (e.g., observed forcing, increased degrees of freedom), we acknowledge the well-known ENSO biases present in GFDL-CM2.1 (Wittenberg et al. 2006). Generally, GFDL-CM2.1 ENSO events are too strong, occur too frequently, and are not clearly seasonally phase locked. The fact that nPOGA exhibits such skill in spite of these model errors is a testament to the robust physical connection between the North and tropical Pacific. However, the possibility that our results may be model dependent cannot be completely ruled out. Therefore, a comprehensive comparison with other realistic models will be important moving forward.

Acknowledgments. D.J.A is supported by the National Science Foundation Graduate Research Fellowship (NSF; DGE-1144086 and 1637450). Y.K. is supported by the Japan Society for the Promotion of Science (18H01278 and 18H01281), the Japan Science and Technology Agency through Belmont Forum CRA "InterDec," and the Japan Ministry of Education, Culture, Sports, Science and Technology through the Integrated Research Program for Advancing Climate Models. S.P.X. and W.Z. are supported by the NSF (1637450). Y.Z. is supported by the China Scholarship Council (201706330016), the National Key Research and Development Program of China (2016YFA0601804), and the National Science Foundation of China (41490640 and 41490641). A.J.M is supported by the NSF (OCE1419306) and the National Oceanic and Atmospheric Administration (NOAA; NA17OAR4310106). We thank Manu Di Lorenzo, Giovanni Liguori, and Dan Vimont (who also served as a referee) for their helpful comments during the course of our study. We further thank two anonymous referees who provided additional

insightful comments that greatly improved the clarity and focus of our results. We also express our gratitude to the World Climate Research Programme's Working Group on Coupled Modelling, which maintains CMIP.

REFERENCES

Alexander, M. A., D. J. Vimont, P. Chang, and J. D. Scott, 2010: The impact of extratropical atmospheric variability on ENSO: Testing the seasonal footprinting mechanism using coupled model experiments. *J. Climate*, **23**, 2885–2901, https://doi.org/10.1175/2010JCLI3205.1.

Amaya, D. J., S. P. Xie, A. J. Miller, and M. J. McPhaden, 2015: Seasonality of tropical Pacific decadal trends associated with the 21st century global warming hiatus. *J. Geophys. Res. Oceans*, **120**, 6782–6798, https://doi.org/10.1002/2015JC010906.

——, N. E. Bond, A. J. Miller, and M. J. Deflorio, 2016: The evolution and known atmospheric forcing mechanisms behind the 2013-2015 North Pacific warm anomalies. US CLIVAR Variations, Vol. 14, No. 2, 1–6, https://indd.adobe.com/view/ffe33cde-3628-42e8-adc2-eaf85d8312e4.

——, M. J. DeFlorio, A. J. Miller, and S. P. Xie, 2017: WES feedback and the Atlantic meridional mode: Observations and CMIP5 comparisons. *Climate Dyn.*, **49**, 1665–1679, https://doi.org/10.1007/s00382-016-3411-1.

Barsugli, J. J., and D. S. Battisti, 1998: The basic effects of atmosphere–ocean thermal coupling on midlatitude variability. *J. Atmos. Sci.*, **55**, 477–493, https://doi.org/10.1175/1520-0469(1998)055<0477:TBEOAO>2.0.CO;2.

Bond, N. A., M. F. Cronin, H. Freeland, and N. J. Mantua, 2015: Causes and impacts of the 2014 warm anomaly in the NE Pacific. *Geophys. Res. Lett.*, **42**, 3414–3420, https://doi.org/10.1002/2015GL063306.

Chang, P., L. Zhang, R. Saravanan, D. J. Vimont, J. C. H. Chiang, L. Ji, H. Seidel, and M. K. Tippett, 2007: Pacific meridional mode and El Niño–Southern Oscillation. *Geophys. Res. Lett.*, **34**, L16608, https://doi.org/10.1029/2007GL030302.

Chiang, J. C. H., and D. J. Vimont, 2004: Analogous Pacific and Atlantic meridional modes of tropical atmosphere–ocean variability. *J. Climate*, **17**, 4143–4158, https://doi.org/10.1175/JCLI4953.1.

Clarke, A. J., 2014: El Niño physics and El Niño predictability. *Annu. Rev. Mar. Sci.*, **6**, 79–99, https://doi.org/10.1146/ANNUREV-MARINE-010213-135026.

Delworth, T. L., and Coauthors, 2006: GFDL's CM2 Global Coupled Climate Models. Part I: Formulation and simulation characteristics. *J. Climate*, **19**, 643–674, https://doi.org/10.1175/JCLI3629.1.

Deser, C., I. R. Simpson, K. A. McKinnon, and A. S. Phillips, 2017: The Northern Hemisphere extratropical atmospheric circulation response to ENSO: How well do we know it and how do we evaluate models accordingly? *J. Climate*, **30**, 5059–5082, https://doi.org/10.1175/JCLI-D-16-0844.1.

Di Lorenzo, E., and N. Mantua, 2016: Multi-year persistence of the 2014/15 North Pacific marine heatwave. *Nat. Climate Change*, **6**, 1042–1047, https://doi.org/10.1038/nclimate3082.

Furtado, J. C., E. Di Lorenzo, B. T. Anderson, and N. Schneider, 2012: Linkages between the North Pacific Oscillation and central tropical Pacific SSTs at low frequencies. *Climate Dyn.*, **39**, 2833–2846, https://doi.org/10.1007/s00382-011-1245-4.

Gill, A. E., 1980: Some simple solutions for heat-induced tropical circulation. *Quart. J. Roy. Meteor. Soc.*, **106**, 447–462, https://doi.org/10.1002/qj.49710644905.

Horel, J. D., and J. M. Wallace, 1981: Planetary-scale phenomena associated with the Southern Oscillation. *Mon. Wea. Rev.*, **109**, 813–829, https://doi.org/10.1175/1520-0493(1981)109<0813:PSAPAW>2.0.CO;2.

Hu, S., and A. V. Fedorov, 2016: Exceptionally strong easterly wind burst stalling El Niño of 2014. *Proc. Natl. Acad. Sci. USA*, **113**, 2005–2010, https://doi.org/10.1073/pnas.1514182113.

——, and ——, 2018: Cross-equatorial winds control El Niño diversity and change. *Nat. Climate Change*, **8**, 798–802, https://doi.org/10.1038/s41558-018-0248-0.

——, and ——, 2019: The extreme El Niño of 2015–2016: The role of westerly and easterly wind bursts, and preconditioning by the failed 2014 event. *Climate Dyn.*, **52**, 7339–7357, https://doi.org/10.1007/S00382-017-3531-2.

Jin, F.-F., 1997: An equatorial ocean recharge paradigm for ENSO. Part I: Conceptual model. *J. Atmos. Sci.*, **54**, 811–829, https://doi.org/10.1175/1520-0469(1997)054<0811:AEORPF>2.0.CO;2.

Kim, H., F. Vitart, and D. E. Waliser, 2018: Prediction of the Madden–Julian oscillation: A review. *J. Climate*, **31**, 9425–9443, https://doi.org/10.1175/JCLI-D-18-0210.1.

Kobayashi, S., and Coauthors, 2015: The JRA-55 Reanalysis: General specifications and basic characteristics. *J. Meteor. Soc. Japan. Ser. II*, **93**, 5–48, https://doi.org/10.2151/JMSJ.2015-001.

Kosaka, Y., and S.-P. Xie, 2013: Recent global-warming hiatus tied to equatorial Pacific surface cooling. *Nature*, **501**, 403–407, https://doi.org/10.1038/nature12534.

Larson, S. M., and B. P. Kirtman, 2014: The Pacific meridional mode as an ENSO precursor and predictor in the North American multimodel ensemble. *J. Climate*, **27**, 7018–7032, https://doi.org/10.1175/JCLI-D-14-00055.1.

——, K. V. Pegion, and B. P. Kirtman, 2018: The South Pacific meridional mode as a thermally driven source of ENSO amplitude modulation and uncertainty. *J. Climate*, **31**, 5127–5145, https://doi.org/10.1175/JCLI-D-17-0722.1.

Levine, A. F. Z., and M. J. McPhaden, 2016: How the July 2014 easterly wind burst gave the 2015–2016 El Niño a head start. *Geophys. Res. Lett.*, **43**, 6503–6510, https://doi.org/10.1002/2016GL069204.

——, ——, and D. M. W. Frierson, 2017: The impact of the AMO on multidecadal ENSO variability. *Geophys. Res. Lett.*, **44**, 3877–3886, https://doi.org/10.1002/2017GL072524.

Li, X., S. P. Xie, S. T. Gille, and C. Yoo, 2016: Atlantic-induced pan-tropical climate change over the past three decades. *Nat. Climate Change*, **6**, 275–279, https://doi.org/10.1038/nclimate2840.

Lin, C.-Y., J.-Y. Yu, and H.-H. Hsu, 2015: CMIP5 model simulations of the Pacific meridional mode and its connection to the two types of ENSO. *Int. J. Climatol.*, **35**, 2352–2358, https://doi.org/10.1002/joc.4130.

Liu, Z., and S. Xie, 1994: Equatorward propagation of coupled air–sea disturbances with application to the annual cycle of the eastern tropical Pacific. *J. Atmos. Sci.*, **51**, 3807–3822, https://doi.org/10.1175/1520-0469(1994)051<3807:EPOCAD>2.0.CO;2.

Lu, F., and Z. Liu, 2018: Assessing extratropical influence on observed El Niño–Southern Oscillation events using regional coupled data assimilation. *J. Climate*, **31**, 8961–8969, https://doi.org/10.1175/JCLI-D-17-0849.1.

——, ——, Y. Liu, S. Zhang, and R. Jacob, 2017: Understanding the control of extratropical atmospheric variability on ENSO using a coupled data assimilation approach. *Climate Dyn.*, **48**, 3139–3160, https://doi.org/10.1007/s00382-016-3256-7.

Ma, J., S. P. Xie, and H. Xu, 2017: Contributions of the North Pacific meridional mode to ensemble spread of ENSO prediction. *J. Climate*, **30**, 9167–9181, https://doi.org/10.1175/JCLI-D-17-0182.1.

Maeda, S., Y. Urabe, K. Takemura, T. Yasuda, and Y. Tanimoto, 2016: Active role of the ITCZ and WES feedback in hampering the growth of the expected full-fledged El Niño in 2014. *SOLA*, **12**, 17–21, https://doi.org/10.2151/SOLA.2016-004.

Martinez-Villalobos, C., and D. J. Vimont, 2017: An analytical framework for understanding tropical meridional modes. *J. Climate*, **30**, 3303–3323, https://doi.org/10.1175/JCLI-D-16-0450.1.

Min, Q., J. Su, and R. Zhang, 2017: Impact of the South and North Pacific meridional modes on the El Niño–Southern Oscillation: Observational analysis and comparison. *J. Climate*, **30**, 1705–1720, https://doi.org/10.1175/JCLI-D-16-0063.1.

Park, J. Y., S. W. Yeh, J. S. Kug, and J. Yoon, 2013: Favorable connections between seasonal footprinting mechanism and El Niño. *Climate Dyn.*, **40**, 1169–1181, https://doi.org/10.1007/s00382-012-1477-y.

Rayner, N. A., D. E. Parker, E. B. Horton, C. K. Folland, L. V. Alexander, D. P. Rowell, E. C. Kent, and A. Kaplan, 2003: Global analyses of sea surface temperature, sea ice, and night marine air temperature since the late nineteenth century. *J. Geophys. Res.*, **108**, 4407, https://doi.org/10.1029/2002JD002670.

Rogers, J. C., 1981: The North Pacific Oscillation. *J. Climatol.*, **1**, 39–57, https://doi.org/10.1002/JOC.3370010106.

Sanchez, S. C., D. J. Amaya, A. J. Miller, S.-P. Xie, and C. D. Charles, 2019: The Pacific meridional mode over the last millennium. *Climate Dyn.*, **53**, 3547–3560, https://doi.org/10.1007/s00382-019-04740-1.

Shin, S. J., and S. I. An, 2018: Interdecadal change in the relationship between the North Pacific Oscillation and the Pacific meridional mode and its impact on ENSO. *Asia-Pac. J. Atmos. Sci.*, **54**, 63–76, https://doi.org/10.1007/s13143-017-0060-1.

Siler, N., Y. Kosaka, S. P. Xie, and X. Li, 2017: Tropical ocean contributions to California's surprisingly dry El Niño of 2015/16. *J. Climate*, **30**, 10 067–10 079, https://doi.org/10.1175/JCLI-D-17-0177.1.

Taylor, K. E., R. J. Stouffer, and G. A. Meehl, 2012: An overview of CMIP5 and the experiment design. *Bull. Amer. Meteor. Soc.*, **93**, 485–498, https://doi.org/10.1175/BAMS-D-11-00094.1.

Vimont, D. J., 2010: Transient growth of thermodynamically coupled variations in the tropics under an equatorially symmetric mean state. *J. Climate*, **23**, 5771–5789, https://doi.org/10.1175/2010JCLI3532.1.

——, D. S. Battisti, and A. C. Hirst, 2001: Footprinting: A seasonal connection between the tropics and mid-latitudes. *Geophys. Res. Lett.*, **28**, 3923–3926, https://doi.org/10.1029/2001GL013435.

——, ——, and ——, 2003a: The seasonal footprinting mechanism in the CSIRO general circulation models. *J. Climate*, **16**, 2653–2667, https://doi.org/10.1175/1520-0442(2003)016<2653:TSFMIT>2.0.CO;2.

——, J. M. Wallace, and D. S. Battisti, 2003b: The seasonal footprinting mechanism in the Pacific: Implications for ENSO. *J. Climate*, **16**, 2668–2675, https://doi.org/10.1175/1520-0442(2003)016<2668:TSFMIT>2.0.CO;2.

——, M. A. Alexander, and A. Fontaine, 2009: Midlatitude excitation of tropical variability in the Pacific: The role of thermodynamic coupling and seasonality. *J. Climate*, **22**, 518–534, https://doi.org/10.1175/2008JCLI2220.1.

——, ——, and M. Newman, 2014: Optimal growth of central and east Pacific ENSO events. *Geophys. Res. Lett.*, **41**, 4027–4034, https://doi.org/10.1002/2014GL059997.

Wittenberg, A. T., A. Rosati, N. C. Lau, and J. J. Ploshay, 2006: GFDL's CM2 global coupled climate models. Part III: Tropical Pacific climate and ENSO. *J. Climate*, **19**, 698–722, https://doi.org/10.1175/JCLI3631.1.

Xie, S.-P., and S. G. H. Philander, 1994: A coupled ocean-atmosphere model of relevance to the ITCZ in the eastern Pacific. *Tellus*, **46A**, 340–350, https://doi.org/10.3402/tellusa.v46i4.15484.

You, Y., and J. C. Furtado, 2017: The role of South Pacific atmospheric variability in the development of different types of ENSO. *Geophys. Res. Lett.*, **44**, 7438–7446, https://doi.org/10.1002/2017GL073475.

Zhang, H., A. Clement, and P. N. DiNezio, 2014a: The South Pacific meridional mode: A mechanism for ENSO-like variability. *J. Climate*, **27**, 769–783, https://doi.org/10.1175/JCLI-D-13-00082.1.

——, C. Deser, A. Clement, and R. Tomas, 2014b: Equatorial signatures of the Pacific meridional modes: Dependence on mean climate state. *Geophys. Res. Lett.*, **41**, 568–574, https://doi.org/10.1002/2013GL058842.

Zhang, L., P. Chang, and L. Ji, 2009: Linking the Pacific meridional mode to ENSO: Coupled model analysis. *J. Climate*, **22**, 3488–3505, https://doi.org/10.1175/2008JCLI2473.1.

Zhang, Y., S. P. Xie, Y. Kosaka, and J. C. Yang, 2018: Pacific decadal oscillation: Tropical Pacific forcing versus internal variability. *J. Climate*, **31**, 8265–8279, https://doi.org/10.1175/JCLI-D-18-0164.1.